Effect of Pressure on Conformational Dynamics in Polyethylene: A Molecular Dynamics Simulation Study

Rishikesh K. Bharadwaj

Systran Federal Corporation, Dayton, Ohio 45431

Richard H. Boyd*

Department of Material Science and Engineering and Department of Chemical and Fuels Engineering, Room 304 122 S. Central Campus Drive, University of Utah, Salt Lake City, Utah 84112

Received March 14, 2000; Revised Manuscript Received June 5, 2000

ABSTRACT: Molecular dynamics simulations have been used to delineate the pressure dependence of conformational dynamics in polyethylene. Chain dynamics have been studied as a function of pressure (0−25 kbar) at 400 K and as a function of temperature (280−450 K) at an elevated pressure of 10 kbar. The volumetric glass transition is found isobarically (10 kbar) at ∼315 K and is considerably elevated from the ∼220 K atmospheric pressure value. On increasing pressure at constant temperature, the system displays several signatures indicative of the vitrification process that are complementary to those previously found to be associated with lowering of temperature. These include a large increase in autocorrelation function relaxation times, divergence of the relaxation times from conformational transition rates, an increase in spatial heterogeneity of the distribution of conformational transition rates over the various bonds, and an increase in self-correlation of the conformational transitions. Isobarically at high pressure (10 kbar), the variation with temperature of the relaxation times associated with the decay of the dipolar autocorrelation function is in accord with dielectric relaxation experiments. Upon lowering the temperature, the relaxation times diverge from the conformation transition rates, an effect also observed at low pressure.

Introduction

Despite experimental inconvenience, there has long been an awareness of the importance of studying relaxation phenomena in polymeric materials using pressure as a variable in addition to temperature. The origin of this interest may be traced at a practical level to the relatively poor understanding of time−temperature−pressure superposition in comparison to the well-known time−temperature superposition and also at a fundamental level to the importance of the free-volume concept in rationalizing the vitrification process. Experimentally, NMR and dielectric spectroscopy, calorimetry, and neutron scattering have been used to study the pressure dependence of relaxation behavior in a variety of polymeric[1−10] and small molecule glass-forming liquids.[11−15]

The use of molecular dynamics (MD) simulations in studying conformational dynamics in polymeric systems has proven to be of value.[16−28] Significant progress has been made toward understanding the atomistic details of the molecular motions accompanying relaxation processes**.** The conformational transitions underlying segmental relaxation can be identified and classified. For example, in polyethylene (PE) where the most simulation work has been done, conformational transitions are to a significant degree locally cooperative in solution[24] and the melt[16,18] and nearly completely so in the glass.[19] In the melt, where ergodicity prevails, all bonds are equivalent, and the transitions are found to be distributed randomly over the bonds. However, it has also been found that as vitrification takes place upon lowering of temperature, the distribution of transitions over the individual bonds becomes very heterogeneous.[18,19] The bonds are no longer equivalent; some experience relatively high conformational transition rates and others very low rates. As a consequence, autocorrelation function (ACF) relaxation times diverge from conformational transition rates as temperature is lowered. Many of the foregoing results are found to be applicable to polymeric systems in general[22,28,29] and are not specific to PE. MD simulation has been applied effectively to pressure effects on relaxation in a bead−spring model for short polymeric chains.[30] So far, all the simulations on higher molecular weight models for real chains where experimental comparison is possible have studied the conformational dynamics at atmospheric pressure. However, the extension of these simulations to studying chain dynamics and relaxation at elevated pressures is relatively straightforward.

In the present work, the effect of pressure on conformational dynamics was addressed by means of MD simulations. Since conformational dynamics have been extensively studied via MD simulation in PE, this polymer was adopted as the system for study. Two pathways were explored: one along an isotherm at 400 K as a function of pressure and the other along an isobar at 10 kbar as a function of temperature. By the former pathway (isothermal pressure dependence) the effect of pressure alone may be addressed independently of thermal effects. The latter pathway (isobaric temperature dependence) allows a more straightforward correlation with experimental results and permits the extraction of activation energies for conformational transitions and relaxation processes which can be compared to those observed at atmospheric pressure.

Simulation Details

The system adopted was the same as the one invoked in a number of previous studies.[17−19,21] It incorporates a single polyethylene chain of 768 $-CH_2-$ centers in a

10.1021/ma0004615 CCC: $19.00 © 2000 American Chemical Society
Published on Web 07/14/2000

Table 1. Potential Functions[a]

function		
C−C bond stretch energy = $^1/_2 k_R(R - R_0)^2$	$k_R = 663$	$R_0 = 1.54$
bond bending energy = $^1/_2 k_\theta(\theta - \theta_0)^2$ −CH_2− (PE)	$k_\theta = 482$	$q_0 = 111.6°$
torsional potential = $^1/_2 V_3(1 + \cos 3\phi) + ^1/_2 V_1(1 + \cos \phi)$	$V_3 = 13.4$	$V_1 = 3.35$
AUA nonbonded potential, Lennard-Jones 6−12[b] −CH_2−	$\epsilon = 0.686$	$R_{min} = 3.940$; $\sigma = 3.510$; $d = 0.42$

[a] Energies in kJ/mol, distances in Å, angles in rad (shown above in deg). The potentials are from ref 17. [b] For the −CH_2− group the potential is of the "AUA" (anisotropic united atom) type, the interaction center is offset form the C atom by the distance = d along the bisector of the C−C−C angle in the direction of the hydrogens; ϵ is the well depth; R_{min} the distance at the minimum; σ is the corresponding distance at the energy zero.

cubic periodic cell. The −CH_2− units utilize the anisotropic united atom representation where the group is a single center at the carbon position, but the nonbonded forces act at a displaced position along the chain valence angle bisector. The force field parameters, recapitulated here in Table 1, have been previously shown to predict a wide range of properties including the equation of state,[17] small molecule penetrant diffusion,[20] and conformational relaxation behavior[18,19] of polyethylene satisfactorily. Explicit reversible integrators[31] were used to solve the equations of motion in the *NPT* (constant particle number, pressure, and temperature) ensemble. A Nose−Hoover thermostat[32] and an Anderson−Hoover barostat[33] were used to control temperature and pressure, respectively. These modifications of the original equations of motion proposed by Anderson, Nose, and Hoover[34] result in a more accurate generation of the isothermal−isobaric ensemble as their phase space averages. The implementation of the modified extended system methods[32,33] as given by Martyna et al.[31] have been followed exactly in the present work. The frequency of fluctuation of the thermostat and barostat were fixed at 1 ps^{-1}, and the equations of motion were integrated with a time step of 1 fs. A cutoff sphere radius of 9.0 Å was used in the evaluation of nonbonded interactions. Long-range corrections to the system pressure and energy were explicitly considered.[35]

The volume−pressure isotherm at 400 K was investigated over the range 0−25 kbar. The volume−temperature isobar was constructed at a pressure of 10 kbar by performing *NPT* simulations at several temperatures in the range 280−450 K. At each pressure/temperature the systems were equilibrated over a period of 3 ns prior to performing sampling runs to ensure that the resulting volumes from the target T and P values were well established. The latter runs were initiated from the preequilibrated configurations over time periods ranging between 5 and 20 ns with the first 1 ns being excluded before data collection. All computations were preformed on IBM RS-6000/370 workstations.

Results and Discussion

Pressure−Volume−Temperature Behavior. The force field parameters used in the present study have been shown to satisfactorily reproduce the pressure−volume−temperature (*PVT*) behavior of polyethylene in the melt.[17] In the present work quite high pressures were included in order to ensure observation of significant effects. These include pressures where polyethylene is crystalline in the desired temperature range, and thus no experimental data exist for the melt. In fact, an advantage of simulations is the ability to address states that are not experimentally accessible.[21] Normally crystallization is not observed in MD simulations of polymers since it is a nucleation and growth process that would require a very large system and very long times,

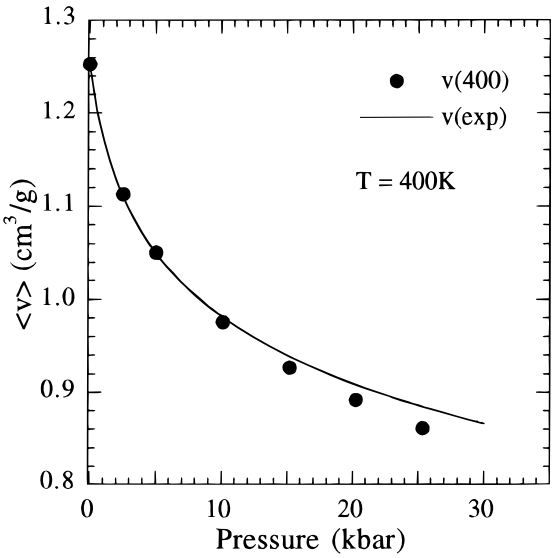

Figure 1. Volume versus pressure behavior at 400 K for bulk polyethylene as determined from MD simulations. The points are from MD simulations. The solid line is the Tait equation representation of the experimental data of Olabisi and Simha (ref 36).

and that is the case here. However, it is useful to extrapolate the available data as some verification of the *PVT* behavior found in simulation. Equation of state data for linear polyethylene[36] are available over pressures of up to 2 kbar in the temperature range 423−476 K. The experimental results presented here include extrapolations, using the Tait equation representation reported[36] of the experimental data to appropriate pressures and temperatures that allow comparison with simulation. The isothermal (400 K) pressure dependence of the time averaged specific volumes are shown in Figure 1. The agreement of the predicted values with the extrapolated experimental data is good over the pressure range studied.

The temperature dependence of the time averaged specific volumes at 10 kbar is shown in Figure 2. The coefficient of thermal expansion in the melt at 10 kbar is found to be 2.2×10^{-4} K^{-1}. This is approximately 3.5 times smaller compared to the experimental[36] value of 7.8×10^{-4} K^{-1} at atmospheric pressure. For comparison, the volume−temperature behavior based on the extrapolation of the experimental data is also shown. The difference between the simulations and the extrapolated experimental data is more apparent on the expanded scale necessary to represent the smaller volume changes effected through temperature variation as opposed to those through pressure. In any event it appears that a realistic representation of the effect of pressure is obtained in simulation.

A break in the volume−temperature curve is seen at ∼315 K. This corresponds to the volumetric glass

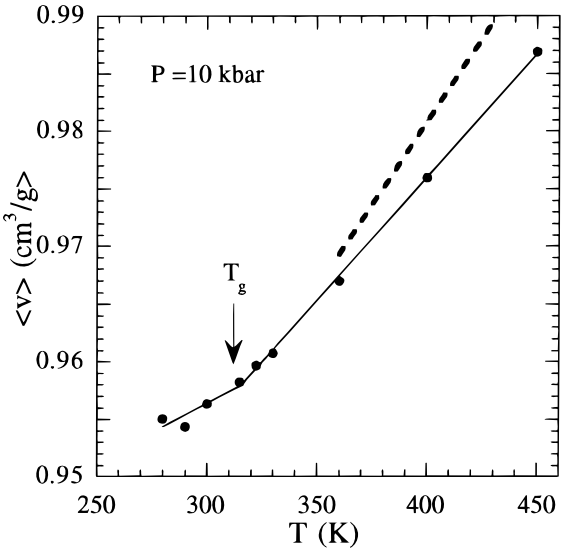

Figure 2. Isobaric volume−temperature dependence at 10 kbar for bulk polyethylene from MD simulations. The points are from MD simulations. The thin solid line is a linear regression fit to the MD data. The thick dashed line is an Tait equation extrapolation of the experimental data of Olabisi and Simha (ref 36).

transition temperature (T_g). Previous MD simulation studies of the same system at atmospheric pressure have located the T_g at ~200[19] and ~225 K.[18] The increase in T_g with increasing pressure is of course expected since increasing the pressure hastens the onset of vitrification by decreasing the free volume.

Effective Torsional Potential. It is useful to start by analyzing an underlying factor that governs the ensuing conformational dynamics. This is the barrier to rotation about the individual bonds making up the chain segments. In a condensed phase the effective barrier to rotation about a bond is the superposition of two contributions. The first is the explicit torsional barrier that is supplied as input in the simulation. The second contribution arises from the nonbonded interactions due to bulk packing. In polyethylene it has been found in simulations at 1 atm that the effective barrier is remarkably insensitive in a statistical sense to packing effects.[19] The effective potential is computed via MD sampling of the torsional angles of all the bonds in the system. Then, from the Boltzmann distribution, the sampled probability $p(\phi)$ of finding a torsional angle at a value, ϕ, is given by

$$p(\phi) = e^{-V(\phi)/kt}/Q \quad (1)$$

where Q is the normalizing partition function and $V(\phi)$ is the effective torsional potential. Inversion leads to

$$V(\phi) = -kT(\ln p(\phi) + \ln Q) \quad (2)$$

Figure 3 shows the pressure dependence (at 400 K) of the effective torsional potential as derived from sampling and the above equation. Also shown is the explicit barrier used in the simulations. Since the comparison is being made at constant temperature, the effects of increasing pressure are probed exclusively. The barrier is threefold in nature with two *gauche* states ($g^{\pm}$) at 60 and 300° and one *trans* (t) state occurring at 180°. In the explicit input potential, the $t \rightarrow g^{\pm}$ barrier is the same as that separating the two *gauche* states. As the pressure is increased, a simultaneous increase

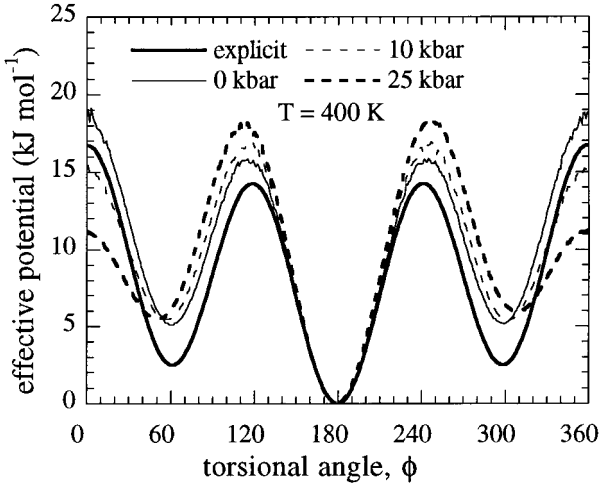

Figure 3. Isothermal pressure dependence (at 400 K) of the effective torsional potential as derived from MD sampling. The explicit torsional potential used in the simulations is also shown.

in the $g^{\pm} \leftrightarrow t$ and lowering of the $g^{\pm} \leftrightarrow g^{\mp}$ barrier may be discerned. The decrease in the $g^{\pm} \leftrightarrow g^{\mp}$ ($\phi = 0°$) barrier is greater than the increase in the $g^{\pm} \leftrightarrow t$ ($\pm 120°$) barrier. This populating of the *cis* conformation at 0° relative to depopulating the eclipsed at 120° may be rationalized in terms of the *cis* being planar and also compact (minimum 1,4 atom separation) in comparison with the 120° eclipsed position. The positions of the *gauche* minima are slightly separated from the *trans* position, with the $g^{\pm}$ occurring at 50° and 310° at 25 kbar. Interestingly, the *gauche* vs *trans* energy difference is relatively insensitive to the increase in pressure. This could well be the result of a tradeoff between the packing efficiency of the planar *trans* conformation and the compactness of the *gauche* with its smaller 1,4 atom separation.

Autocorrelation Function Relaxation. In previous MD simulation work on PE[19] the dipolar autocorrelation (DACF) has played an important role in the interpretation and validation of MD results since relevant experimental data on dipole decorated PE are available. That is the case here as well since there are data available on the effect of pressure on dielectric relaxation in PE.[2]

In general, it can be said that at high temperatures in the melt polymeric segmental relaxation results in a single relaxation process. As temperature is lowered, a bifurcation takes place, and two resolved relaxation regions are observed. The slower, lower frequency branch is associated with longer range segmental motion and is highly temperature dependent (the glass transition, "alpha" process branch). The faster, higher frequency branch is associated with more localized chain motions and is less temperature dependent (the subglass relaxation, "beta" process branch). In PE it has been found that the MD simulations follow the subglass branch as temperature is lowered from the largely merged high-temperature region.[19] The very long simulation times necessary to resolve the two regions have so far prevented the simultaneous observation of both processes isothermally.

The available dielectric data are for semicrystalline linear PE that is decorated sparsely with carbonyl dipoles. In PE the highest temperature ("alpha") relaxation takes place in the crystals, and thus the amorphous fraction glass transition region nomenclature

defaults to "beta". In general, in semicrystalline polymers this latter region is tremendously broadened compared to that in the completely amorphous state.[37] Thus, it can be hard to detect, and its properties are less relevant to the behavior of the analogous region in completely amorphous polymers. However, this is not the case for the amorphous phase subglass region (the "gamma" region by default). No doubt due to the shorter range of the segmental rearrangements, the subglass relaxation in a semicrystalline polymer is very similar to that in the wholly amorphous counterpart in the cases where both states are available.[37] Thus, it is appropriate to compare, within the limitations of some effect of the carbonyl groups on chain dynamics, the experimental subglass relaxation branch in semicrystalline PE with the MD simulations on the amorphous state.

The dipolar autocorrelation function (DACF) is defined as

$$f_{\mathbf{m}}(t) = \langle \mathbf{m}(0)\cdot\mathbf{m}(t)\rangle/m^2 \qquad (3)$$

where **m** represents a virtual unit dipole along the HCH bisector. The moment **m** in eq 3 is correlated only with itself, but the brackets represent ensemble averages over all dipoles (placed at every CH_2 group) in the system. This device is useful in comparing simulation results with experiments on dilute dipole decorated polyethylenes. In addition, the torsional angle autocorrelation function (TACF) was computed. It is defined as

$$f_{\phi}(t) = \frac{\langle \cos\phi(0)\cos\phi(t)\rangle - \langle\cos\phi(0)\rangle^2}{\langle\cos\phi(0)^2\rangle - \langle\cos\phi(0)\rangle^2} \qquad (4)$$

where ϕ represents the value of the torsional angle and the brackets denote ensemble averaging over all torsions in the system. The practice of initiating the calculation of the ACFs from multiple origins (200 ps apart) in the original simulation trajectory was employed to yield an averaged ACF.

The dipolar ACFs from both the 400 K isotherm at various pressures and the 10 kbar isobar at various temperatures are displayed in Figure 4. The ACFs were fit by the Kohlrausch−Williams−Watts[38] (KWW) stretched exponential given by

$$f(t) = \mathrm{e}^{-(t/\tau)^{\beta}} \qquad (5)$$

where τ represents a central relaxation time and β a width parameter. The KWW fits to the dipolar ACFs are also shown in Figure 4.

The pressure dependence of the relaxation times and the β width parameter as obtained from the KWW fits to both the dipolar and torsional ACFs at 400 K are shown in Figure 5. It may be seen that the width parameters, especially for the dipolar ACFs, are relatively insensitive to pressure. This circumstance indicates that isothermal superposition shifting among the various pressures along the log t axis would be a realistic procedure. The dependence on pressure for the ACFs is linear, and the DACF results are fit well by the relation

$$-\log\tau = 1.82 - 0.106P\ (\text{kbar}) \qquad (6)$$

The result for the torsional relaxation times is very similar. In general, both polymeric[6−8] and small molecule glass forming liquids[11−13] display a complicated

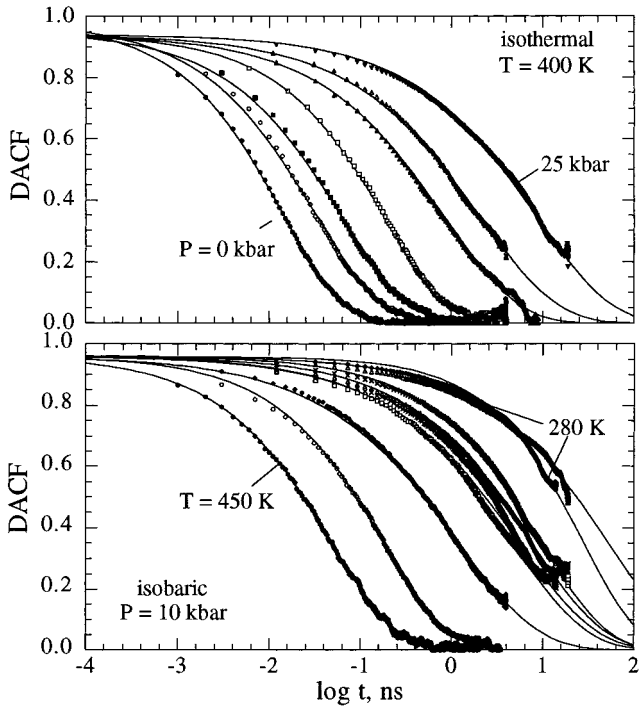

Figure 4. Dipolar autocorrelation functions from MD simulation. Lower panel shows 10 kbar isobaric results at the temperatures (left to right) of 450, 400, 360, 330, 322.5, 315, 300, 290, and 280 K. Upper panel is for isothermal results at pressures (left to right) of 0, 2.5, 5, 10, 15, 20, and 25 kbar.

and varied behavior in their isothermal pressure dependence of relaxation times or viscosity. The relation in eq 6 can be considered analogous to Arrhenius temperature dependence if pressure variation is regarded as an inverse of temperature variation. Conversely, in some systems the pressure dependence can be nonlinear analogous to Vogel−Fulcher (VF)[39] temperature dependence but where temperature is replaced by inverse pressure.

The activation volume, ΔV^*, computed from eq 6, where $-\log\tau$ plays the role of a rate constant, and the relation, in which ΔG^* is the free energy of activation,

$$\left(\frac{\partial \ln k_{\text{rate}}}{\partial P}\right)_T = -\left(\frac{\partial \Delta G^*}{\partial P}\right)_T/RT = -\Delta V^*/RT \qquad (7)$$

is found to be 8.1 $\text{cm}^3\ \text{mol}^{-1}$. This value is compared to experimental values from dielectric measurements at lower temperature[2] in Figure 6. Although the precision of the experimental values is not high, a trend of decreasing values with increasing temperature is seen that seems consistent with a lower value from simulation at much higher temperature.

The experimental dielectric data reported[2] were taken isochronally (at 10 Hz, 100 Hz, 1 kHz, and 10 kHz) as a function of temperature along five isobars (0, 2.1, 2.8, 3.5, and 4.2 kbar). This results in a set of four log $f_{\max}$, $T_{\max}$ values (i.e., a loss map) for each of the five isobars. In addition, we have constructed here an approximate loss map at 10 kbar by extrapolation of the $T_{\max}$ values for each isochrone vs pressure. The log $f_{\max}$ values were converted to KWW relaxation times, τ, via the relation $\omega_{\max}\tau = 1$, where $\omega_{\max} = 2\pi f_{\max}$, that prevails closely for inversions of the KWW relaxation function to the frequency domain.[19]

The isobaric temperature dependence at 10 kbar of the MD KWW dipolar relaxation times is shown in

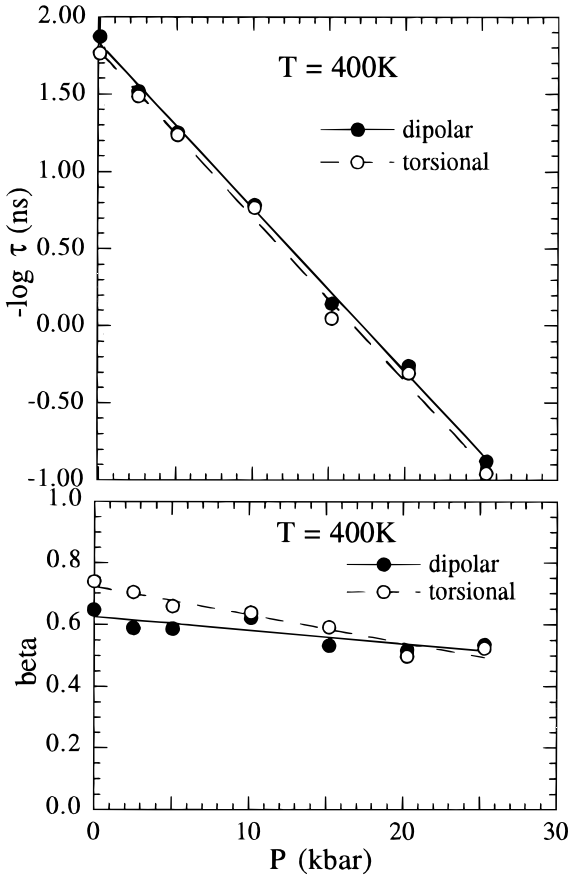

Figure 5. Upper panel: isothermal (400 K) pressure dependence of the KWW relaxation times for the dipolar and torsional autocorrelation functions. Lower panel: the KWW width parameters corresponding to the relaxation times. The curves are linear fits to the MD data.

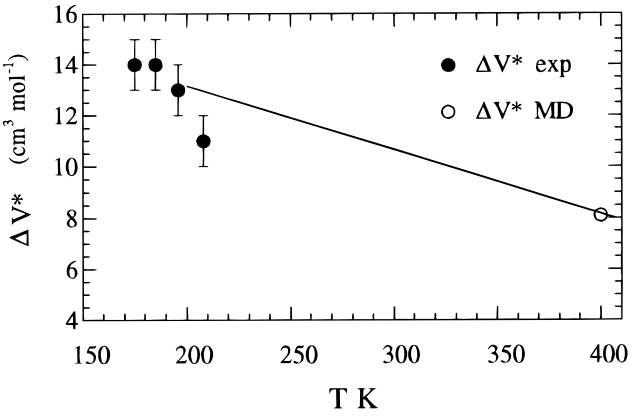

Figure 6. Activation volume from pressure dependence of relaxations times. Filled points with error bars are from experimental dielectric data (ref 2). Open circle is the MD result at 400 K (Figure 5). The line serves to connect the temperature regions of the simulation and the experiments.

Figure 7 as $-\log \tau$ vs $1/T$. MD data from previous simulations at atmospheric pressure are displayed as well.[19] Also shown are experimental results,[2] constructed as described above, for 10 and 4.2 kbar. MD results for the torsional ACF are quite similar and are not shown.

It is apparent in Figure 7 that there is a considerable gap in relaxation times between the time scales of the simulations at 10 kbar and the corresponding experimental data. It was previously noted at atmospheric

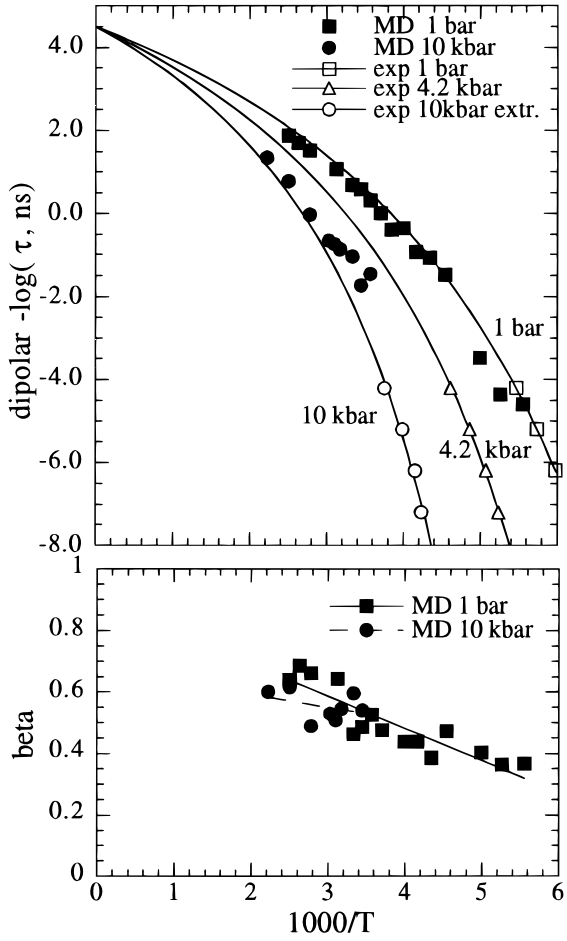

Figure 7. Upper panel: isobaric temperature dependence of the KWW relaxation times for the dipolar autocorrelation function. Filled circles are from MD simulation in this work at 10 kbar. The filled squares are form MD simulation at 1 atm from Jin and Boyd (ref 19). Open squares and triangles are experimental results of Sayre et al. (ref 2); the open circles are extrapolation of experimental results to 10 kbar. The curves are fits of the constrained VF relation, eq 8, to the experimental results: 1 bar, $A = 725.7$, $T_0 = 99.4$; 4.2 kbar, $A = 861.3$, $T_0 = 116.9$; 10 kbar, $A = 1007.8$, $T_0 = 148.3$. Lower panel: MD KWW width parameters corresponding to the relaxation times. The curves are linear fits.

pressure[18,19] that the MD relaxation times obey a nearly Arrhenius temperature dependence at lower temperatures. However, when the complete temperature range is considered, including the higher temperature merged (α, β) region (β, γ in PE), the overall merged process and the MD *subglass* branch can be jointly represented *empirically* by a function of the V−F *form*. This observation may well be peculiar to PE where the subglass process is exceptionally strong compared to the glass transition branch and probably has no implication with respect to the customary use of the V−F function to jointly represent the merged (α, β) region and the resolved α branch. However, invocation of this form is useful in connecting the low-temperature experimental region to the higher temperature region of the MD 10 kbar results. Key to the extrapolation adopted is the premise that there is a finite high-temperature limit of the relaxation times and that this limit is of the order of multiple femtoseconds.[40] That is, the time scale of molecular or "phonon-like" vibrations is approached as the limit. The three solid curves in Figure 7 are fits of the VF relation to the experimental data displayed under the constraint that the high-temperature limit

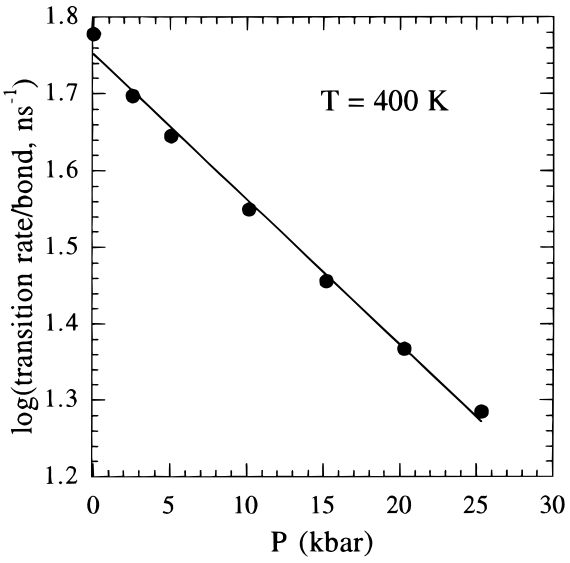

Figure 8. Pressure dependence of the conformational transition rates at 400 K for bulk polyethylene.

to the relaxation times is 30 fs,[40] or

$$-\log \tau = 4.5 - A/(T - T_0) \qquad (8)$$

where τ is in nanoseconds. The A and T_0 parameter values are given in Figure 7.

It may be seen in Figure 7 that a reasonable correspondence is found between the experimental and MD relaxation times. The results at high pressure show an obvious shift to longer relaxation times and higher slope and activation energy compared to those at atmospheric pressure.

Figure 7 also displays the MD KWW β width parameters for 1 bar and 10 kbar. At atmospheric pressure the width parameters indicate significant broadening of the relaxation process as temperature is lowered over a wide range. Although the temperature range is limited, the results at 10 kbar are similar to those at low pressure and confirm the relative lack of effect of pressure on the relaxation width observed in Figure 5.

Conformational Transition Rates. The definition and computation of conformational transitions follows previous work closely[18,19,21] and is therefore described only briefly here. A conformational transition is deemed to have taken place when a bond changes its torsional state from one minimum, traverses a barrier, and comes within ±5° of another minimum. The conformational transition rate is obtained from the slope of the linear curve obtained by plotting the number of transitions versus time and is expressed as the number of transitions per bond per ns. The logarithm of the conformational transition rates exhibits a linear dependence with pressure as shown in Figure 8. The activation volume computed from the slope in Figure 8 is 1.45 cm^3 mol^{-1}. The isobaric temperature dependence of the conformational transition rates at 10 kbar is also linear with an activation energy of 15.4 kJ mol^{-1} as shown in Figure 9. Also shown in Figure 9 are results from previous simulations at atmospheric pressure.

The difference in the effects of both temperature and pressure on conformational transition rates in comparison to their effects on autocorrelation function relaxation times is striking. It has previously been noted[18,19] that, at 1 atm, the transition rates remain Arrhenius with decreasing temperature whereas ACF relaxation

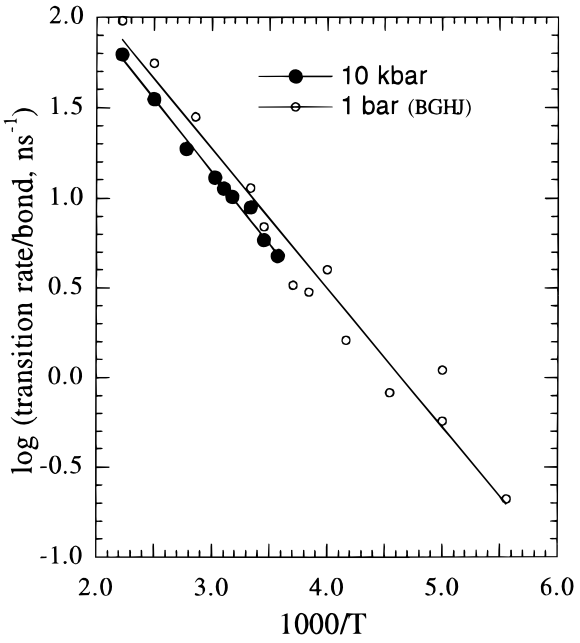

Figure 9. Temperature dependence of the conformational transition rates at 10 kbar for bulk polyethylene (filled circles). Also shown (open circles) are results at 1 atm from Boyd, Gee, Han, and Jin (ref 18).

times show V−F behavior as temperature is lowered (cf. Figures 7 and 9 at 1 bar). The activation energy for transitions (∼15 kJ mol^{-1}) corresponds to a single barrier height in the explicit torsional potential, but only at the high temperature limit does this prevail for the ACF behavior. The transition rates and relaxation times diverge as temperature is lowered. In the present case, pressure is also found to have a very different effect on the transition rates compared to the ACF relaxation times. In Figure 8 it is seen that pressure has only a modest influence on the transition rates but a much greater influence of pressure on the ACF relaxation times is seen in Figure 5. It is also observed, in Figure 9, that Arrhenius temperature variation of transition rates is maintained with the single barrier value of the activation energy. This is the same circumstance as prevails at low pressure (1 bar).

A further comment on the similarity of the high- and low-pressure results for the transition rates is in order. The fact that the *gauche*−*gauche* and *gauche*−*trans* barriers in the effective potential in Figure 3 have a noticeable change with pressure might be thought to result in more difference in the transition rates at high and low pressure in Figure 9. However, one barrier is decreased and the other increased, and it appears that the effects compensate each other.

The differences in ACF relaxation time vs transition rate behavior as a function of temperature have previously been rationalized in terms of the following picture.[18,19] At high temperature in the melt the system is ergodic. Each bond is equivalent, and torsional space is visited ergodically by each bond according to the Boltzmann distribution as indicated in Figure 3. The lifetimes at any point along the effective potential are relatively short. The conventional transition state theory (TST) picture prevails, and conformational transitions take place as initiated from one potential minimum, the barrier is crossed, and the final state is reached at another minimum. Although a significant degree of local correlation of bond jumps is observed, the barrier

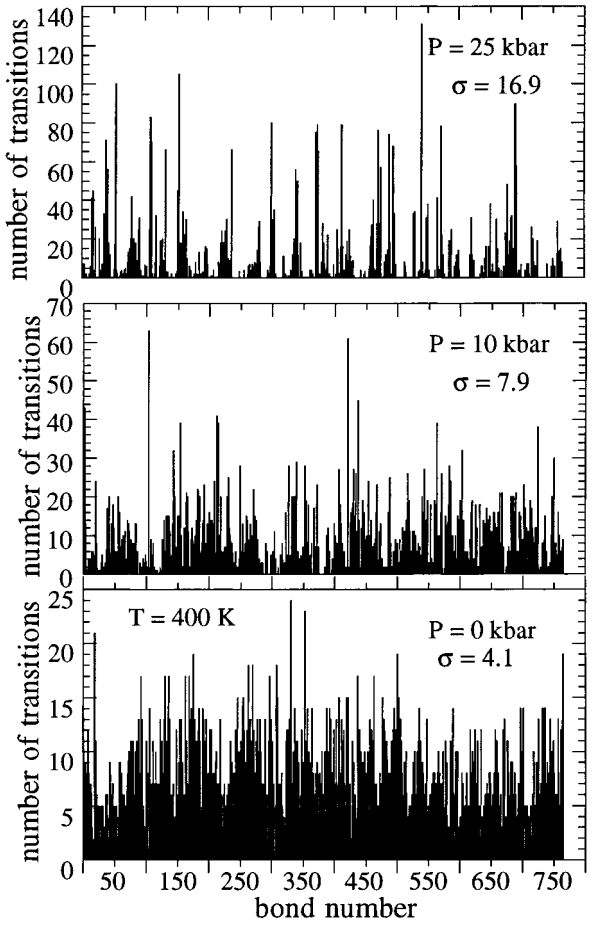

Figure 10. Distribution of conformational transitions among the bonds, as numbered serially along the chain, as a function of applied pressure at 400 K. The standard deviation of the distributions is also shown. A total of 5000 transitions were considered at each pressure.

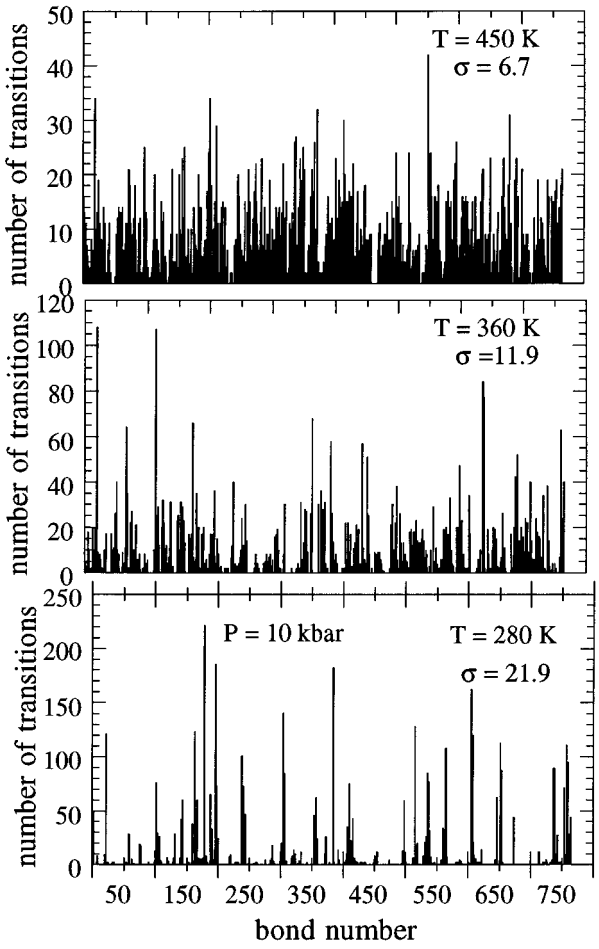

Figure 11. Distribution of conformational transitions among the bonds in the system as a function of temperature at 10 kbar. The standard deviation of the distributions is also shown. A total of 5000 transitions were considered at each temperature.

crossings are sequential rather than simultaneous. The activation energy corresponds to a single barrier. These transitions cause the ACF to relax in a similar fashion, with a single barrier activation energy. However, as temperature is lowered, ergodicity no longer prevails on the time scale of experiments. The bonds now become nonequivalent. The lifetimes at a point on the effective potential become long enough that a given bond is not to be considered as undergoing torsional oscillation about the minimum in the effective potential but rather undergoing oscillations about the point in the effective potential where the bond finds itself for a long time. In the TST picture transitions are initiated from this point and are completed to another point not necessarily at the minimum in the effective potential. Thus, a wide distribution of activation energies appears depending on the points on the effective potential involved. Some bonds make many more transitions than others. Although the transitions at the high rate bonds can cause those bonds to make a completely relaxed contribution to the ACF relaxation, the low rate bonds may not contribute at all over an extended time period. Since the ACF is a system average, the ACF decays more slowly than indicated by the transition rates. This heterogeneity in transition rates is easily detected in the simulations and is taken up in the next section. The observation that the transition rates remain at the barrier value is more problematic, but one explanation is that there is a compensatory effect between the higher rates from decreased barriers at a high-energy point on the torsional potential and the decreased probability of being at the higher energy point.[18]

The effects of pressure on transition rates and ACF decay observed are consistent with the effects of temperature discussed above. Increase of pressure isothermally also results in the onset of nonergodicity and the attendant nonequivalence of the bonds. This has a pronounced effect on the ACF decay through the onset of heterogeneity in bond transition rates but less so on the overall transition rates.

Spatial Distribution of Conformational Transitions. The distribution of a fixed total number of transitions (5000) among the individual bonds, the latter numbered serially along the chain, is shown in Figure 10 as a function of pressure at 400 K and in Figure 11 as a function of temperature at 10 kbar. To aid in quantitative comparison, the standard deviation of the resulting distributions is shown. For a random distribution of transitions over the bonds a Poisson distribution should prevail; the standard deviation should be $X^{1/2}$, where X is the average number of transitions per bond ($X = 5000/765 = 6.53$; $X^{1/2} = 2.55$). In the isothermal pressure dependence (Figure 10), the spatial distribution becomes increasingly heterogeneous with increasing pressure. This is evident both visually and by noting that the standard deviations for the distributions diverge increasingly from the Poisson value with increas-

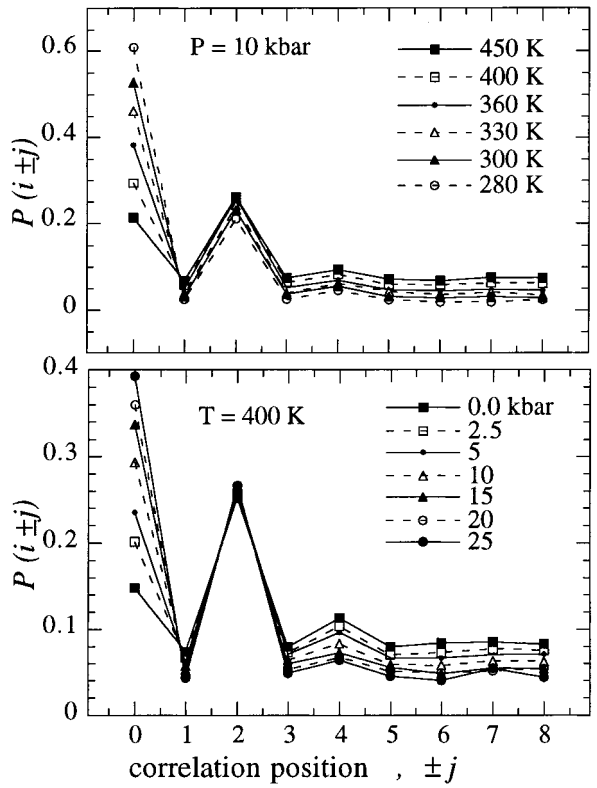

Figure 12. Local chain cooperativity. The probability that a jump at bond i is followed by a jump at $\pm j$ where j is restricted to a window of ±8 bonds. The lines serve to connect the points for clarity. Lower panel shows results at different values of applied pressure at 400 K; upper panel shows results at different temperatures at 10 kbar.

ing pressure. A similar situation prevails in the isobaric temperature dependence (Figure 11) where the heterogeneity is seen to set in well above the MD volumetric T_g (~315 K). The application of an external pressure of 10 kbar appears to hasten the onset of the vitrification process as is amply evidenced by the conformational heterogeneity. The emergence of conformational heterogeneity seems to be an universal signature of a vitrifying bulk polymeric system.[18,19,21,22,28,29] The same heterogeneity is also realized in the isothermal pressure dependence at high pressures, giving further evidence that the system is in or approaching the glassy state.

Local Correlation of Transitions. It has been found that there is significant correlation between conformational transitions in bulk PE melt and glass.[16,18,19] That is, it can be that a transition at a given bond is followed by a transition at another bond in the immediate vicinity with greater or less probability than random. If so, local chain correlation of transitions is said to exist. Correlation is conveniently investigated via a hazard plot. The conformational transitions are listed in chronological order of occurrence along with the location at which they occurred. If bond i undergoes a conformational transition, the next bond j that undergoes a transition within a fixed window of ±8 bonds is tracked. A distribution of these correlation events is constructed and is expressed as a probability, $p(i\pm j)$, of finding a correlated event at a position $\pm j$ from the initiating bond. Previous studies[16,18,19] have found the presence of significant ±2 correlation in bulk polyethylene in the melt even though uncorrelated events are the most common. In addition, the transitions became increasingly self-correlated (±0) as the temperature is lowered from the melt to the glass region. That is, events where a bond jumps back to its original state before another nearby jump occurs become increasingly prevalent. In the glass essentially all transition events are either ±2 next neighbor correlated or ±0 self-correlated. It is the self-correlated transitions that are largely responsible for the maintenance of the transiton rates as Arrhenius in nature with modest activation energy, a situation discussed in the section above on transition rates.

The results of the correlation behavior are shown in Figure 12 and for the isothermal pressure and isobaric temperature dependence. These results are similar to the observations from previous studies. A strong tendency for ±2 correlation is seen. As the pressure is increased or the temperature is lowered, self-correlated transitions become increasingly frequent. This is further manifestation of the complementary effects of temperature and pressure.

Conclusions

Conformational dynamics in polyethylene have been probed as a function of pressure. Two scenarios were considered wherein the glassy state is attained by increasing the applied pressure at constant temperature (400 K) and secondly by lowering the temperature at constant pressure (10 kbar). Not surprisingly, it is found that the nature of the conformational dynamics at elevated pressure mimics that at low temperatures. As pressure is increased isothermally, several trademark features of vitrification are observed. These include the divergence of ACF relaxation times from conformation transition rates, the increase in spatial heterogeneity of conformational transitions, and an increase in ±0 self-correlation of the conformational transitions. Isothermal superposition of the dipolar ACFs among the various pressures is observed, but isobarically the relaxation widths increase noticeably with decreasing temperature.

Acknowledgment. R.K.B. is grateful to the Materials and Manufacturing Directorate, Air Force Research Laboratory (WPAFB), for financial support. R.H.B. is indebted to the Polymers Program, Division of Materials Research, National Science Foundation, for support of this work. R.K.B. dedicates this article to the memory of Uday Narayan Nayak.

References and Notes

(1) Williams, G.; Watts, D. C. In *Dielectric Properties of Polymers*; Karasz, F. E., Ed.; Plenum Press: New York, 1972; Chapter 2.
(2) Sayre, J. A.; Swanson, S. R.; Boyd, R. H. *J. Polym. Sci., Part B: Polym. Phys.* **1978**, *16*, 1739.
(3) Starkweather, H. W.; Avakian, P.; Fontanella, J. J.; Wintersgill, M. C. *Macromolecules* **1992**, *25*, 7145.
(4) Kulik, A. S.; Prins, K. O. *Polymer* **1994**, *35*, 2307.
(5) Kulik, A. S.; Prins, K. O. *Polymer* **1993**, *34*, 4629. (b) Kulik, A. S.; Prins, K. O. *Polymer* **1993**, *34*, 4635. (c) Kulik, A. S.; Prins, K. O. *Polymer* **1993**, *34*, 4642.
(6) Andersson, S. P.; Andersson, O. *Macromolecules* **1998**, *31*, 2999.
(7) Moura-Ramos, J. J.; Williams, G. *Polymer* **1991**, *32*, 909.
(8) McMullin, G.; Scaife, W. G.; Zentel, R. *Liq. Cryst.* **1995**, *18*, 529.
(9) Floudas, G.; Reisinger, T. *J. Chem. Phys.* **1999**, *111*, 5201.
(10) Cheng, Z.-Y.; Gross, S.; Su, J.; Zhang, Q. M. *J. Polym. Sci., Part B: Polym. Phys.* **1999**, *37*, 983.
(11) Paluch, M.; Hensel-Bielowka, S.; Ziolo, J. *J. Chem. Phys.* **1999**, *110*, 10978.

(12) Paluch, M.; Rzoska, S. J.; Habdas, P.; Ziolo, J. *J. Phys.: Condens. Matter* **1998**, *10*, 4131.
(13) Schig, K. U.; King, H. E.; Bohmer, R. *J. Chem. Phys.* **1998**, *109*, 1472.
(14) AlbaSimionesco, C.; Fujimori, H.; Morineau, D.; Frick, B. *Prog. Theor. Phys.* **1997**, *126*, 229.
(15) Tolle, A.; Schober, H.; Wuttke, J.; Randl, O. G.; Fujara, F. *Phys. Rev. Lett.* **1998**, *80*, 2374.
(16) (a) Rigby, D.; Roe, R. J. *J. Chem. Phys.* **1987**, *87*, 7285. (b) Rigby, D.; Roe, R. J. *J. Chem. Phys.* **1988**, *89*, 5280. (c) Rigby, D.; Roe, R. J. *Macromolecules* **1989**, *22*, 2259. (d) Rigby, D.; Roe, R. J. *Macromolecules* **1990**, *23*, 5312. (e) Rigby, D.; Roe, R. J. In *Computer Simulation of Polymers*; Roe, R. J., Ed.; Prentice Hall: New York, 1991; Chapter 6. (f) Takeuchi, H.; Roe, R. J. *J. Chem. Phys.* **1991**, *94*, 7446. (g) Takeuchi, H.; Roe, R. J. *J. Chem. Phys.* **1991**, *94*, 7458.
(17) Pant, P. V. K.; Han, J.; Smith, G. D.; Boyd, R. H. *J. Chem. Phys.* **1993**, *99*, 597.
(18) Boyd, R. H.; Gee, R. H.; Han, J.; Jin, Y. *J. Chem. Phys.* **1994**, *101*, 788.
(19) Jin, Y.; Boyd, R. H. *J. Chem. Phys.* **1998**, *108*, 9912.
(20) Pant, P. V. K.; Boyd, R. H. *Macromolecules* **1993**, *26*, 679.
(21) Gee, R. H.; Boyd, R. H. *Comput. Theor. Polym. Sci.* **1998**, *8*, 93.
(22) Gee, R. H.; Boyd, R. H. *J. Chem. Phys.* **1994**, *101*, 8028.
(23) Kim, E.-G.; Mattice, W. L. *J. Chem. Phys.* **1994**, *101*, 6242.
(24) (a) Helfand, E.; Wasserman, Z. R.; Weber, T. *Macromolecules* **1980**, *13*, 526. (b) Helfand, E. *J. Chem. Phys.* **1971**, *54*, 4651.
(25) (a) Adolf, D. B.; Ediger, M. D. *Macromolecules* **1991**, *24*, 5834. (b) Adolf, D. B.; Ediger, M. D. *Macromolecules* **1992**, *25*, 1074.
(26) Smith, G. D.; Yoon, D. Y.; Zhu, W.; Ediger, M. D. *Macromolecules* **1994**, *27*, 5563.
(27) Paul, W.; Yoon, D. Y.; Smith, G. D. *Macromolecules* **1994**, *27*, 5563.
(28) Antoniadis, S. J.; Samara, C. T.; Theodorou, D. N. *Macromolecules* **1998**, *31*, 7944.
(29) Bharadwaj, R. K; Boyd, R. H. *J. Chem. Phys.* **1999**, *110*, 10203.
(30) Benneman, C.; Paul, W.; Baschnagel, J.; Binder, K. *J. Phys.: Condens. Matter* **1999**, *11*, 2179.
(31) Martyna, G. J.; Tuckerman, M. E.; Tobias, D. J.; Klien, M. L. *Mol. Phys.* **1996**, *87*, 1117.
(32) Martyna, G. J.; Tuckerman, M. E.; Klein, M. L. *J. Chem. Phys.* **1992**, *97*, 2635.
(33) Martyna, G. J.; Tobias, D. J.; Klien, M. L. *J. Chem. Phys.* **1994**, *101*, 4177.
(34) (a) Andersen, H. C. *J. Chem. Phys.* **1980**, *72*, 2384. (b) Nose, S. *J. Chem. Phys.* **1984**, *81*, 511. (c) Hoover, W. G. *Phys. Rev. A* **1985**, *31*, 1695.
(35) Allen, M.; Tildesley, D. *Computer Simulation of Liquids*; Clarendon Press: Oxford, 1987.
(36) Olabisi, O.; Simha, R. *Macromolecules* **1975**, *8*, 206.
(37) Boyd, R. H. *Polymer* **1985**, *26*, 323.
(38) (a) Kohlrausch, R. *Prog. Ann.* **1847**, *12*, 393. (b) Williams, G.; Watts, D. C. *Trans. Faraday Soc.* **1970**, *66*, 80. (c) Williams, G.; Watts, D. C.; Dev, S. B.; North, A. *Trans. Faraday Soc.* **1971**, *67*, 1323.
(39) (a) Vogel, H. *Phys. Z.* **1921**, *22*, 645. (b) Fulcher, G. S. *J. Am. Chem. Soc.* **1925**, *8*, 339. (c) Fulcher, G. S. *J. Am. Chem. Soc.* **1925**, *8*, 789.
(40) Angell, C. A. *Polymer* **1997**, *38*, 6261.

MA0004615